

# PCCP

Accepted Manuscript



This is an *Accepted Manuscript*, which has been through the Royal Society of Chemistry peer review process and has been accepted for publication.

*Accepted Manuscripts* are published online shortly after acceptance, before technical editing, formatting and proof reading. Using this free service, authors can make their results available to the community, in citable form, before we publish the edited article. We will replace this *Accepted Manuscript* with the edited and formatted *Advance Article* as soon as it is available.

You can find more information about *Accepted Manuscripts* in the [Information for Authors](#).

Please note that technical editing may introduce minor changes to the text and/or graphics, which may alter content. The journal's standard [Terms & Conditions](#) and the [Ethical guidelines](#) still apply. In no event shall the Royal Society of Chemistry be held responsible for any errors or omissions in this *Accepted Manuscript* or any consequences arising from the use of any information it contains.

## ARTICLE

# Unexpected efficiency boosting in CO<sub>2</sub>-microemulsions: A cyclohexane depletion zone near the fluorinated surfactants evidenced by a systematic SANS contrast variation study

Cite this: DOI: 10.1039/x0xx00000x

Received 00th January 2012,  
Accepted 00th January 2012

DOI: 10.1039/x0xx00000x

www.rsc.org/

Y. Pütz<sup>a</sup>, L. Grassberger<sup>a</sup>, P. Lindner<sup>b</sup>, R. Schweins<sup>b</sup>, R. Strey<sup>a</sup> and T. Sottmann<sup>\*c</sup>

Microemulsions with supercritical CO<sub>2</sub> are promising alternatives for organic solvents, especially if both polar and non-polar components need to be dissolved. However, only fluorinated surfactants, which are known to be environmentally unfriendly, are appropriate to formulate well-structured microemulsions. While most approaches to increase the environmental performance of CO<sub>2</sub>-microemulsions deal with the design of new surfactants with a reduced degree of fluorination, we discovered that the partial substitution of CO<sub>2</sub> by cyclohexane enables a considerable reduction of fluorinated surfactants. Thereby the most efficient solubilization of the CO<sub>2</sub>/cyclohexane mixture, which turned out to be pressure-dependent, was found at a cyclohexane-to-CO<sub>2</sub> mass ratio between 1:6 and 1:4. In order to elucidate this unexpected effect a systematic small angle neutron scattering contrast variation study was performed. The analysis of the recorded scattering curves by the *Generalized Indirect Fourier Transformation* clearly shows that the scattering length density profiles differ considerably from scCO<sub>2</sub>-microemulsions without cyclohexane. Instead of a nearly constant scattering length density, a density profile that varies systematically over half of the droplet radius was detected. These results clearly indicate that the observed efficiency boosting is caused by the formation of a depletion zone of cyclohexane close to the fluorinated amphiphilic film.

## A Introduction

Supercritical CO<sub>2</sub> (scCO<sub>2</sub>) has attracted increasing attention in recent years because of its potential as a possible replacement for organic solvents, as it is cheap, nontoxic, non-flammable and environmentally friendly. It was shown first in 1978 by Hubert and Vitzthum that supercritical gases and especially scCO<sub>2</sub> is highly appropriate for the extraction of natural products<sup>1</sup>. As its critical point is easily accessible (31°C and 73 bar), the solvent power can be influenced via density and thus via pressure and temperature. These tunable solvents<sup>2, 3</sup> can be applied in various fields like for example enzymatic catalysis<sup>4</sup> or the synthesis of nanoparticles<sup>5, 6</sup>. In many industrial processes CO<sub>2</sub> is already used routinely<sup>7</sup>, the perhaps best known process being the decaffeination of coffee<sup>8</sup>. However, CO<sub>2</sub> is a very poor solvent for polar substances and such of high molecular weight, which is why emulsions and microemulsions are of interest for applications in which both polar and non-polar substances need to be dissolved. By combining the interesting features of CO<sub>2</sub> and microemulsions via formulation of supercritical microemulsions it is possible to change the properties of the microemulsion without changing the molecular composition, which makes supercritical microemulsions also interesting to fundamental research.

Starting from classical microemulsions using commercially available surfactants Consani and Smith showed that most of these are not compatible with CO<sub>2</sub><sup>9</sup>. This was verified later, showing that for example 40 wt% of a technical grade *n*-alkyl polyglycoether

surfactant is needed to formulate a CO<sub>2</sub>-microemulsion containing equal amounts of brine and CO<sub>2</sub><sup>10</sup>. That fluorinated surfactants are more appropriate to solubilize CO<sub>2</sub> in water and vice versa was found by Beckman *et al.*, who utilized a fluorinated version of sodium bis(2-ethylhexyl) sulfosuccinate (AOT)<sup>11</sup>. In the last decade the properties of different types of CO<sub>2</sub>-microemulsions stabilized by fluorinated surfactants have been investigated, most studies dealing with the formulation of water-in-CO<sub>2</sub> (w/c) microemulsions<sup>12</sup>. The first ones to reveal the microstructure of w/c microemulsions were Eastoe *et al.* who performed high pressure SANS experiments<sup>13</sup>. Since then research on these promising microemulsion systems has spread and numerous publications deal with their microstructure<sup>14-16</sup>, the influence of cosurfactants<sup>17</sup>, formation kinetics<sup>18</sup> or with the design and synthesis of new fluorinated surfactants<sup>19, 20</sup>. Very recently, the kinetics of structural changes in a c/w microemulsion was investigated with time-resolved SANS using a newly designed stroboscopic high-pressure cell<sup>21</sup>. However, since fluorinated surfactants are expensive, non-biodegradable and therefore environmentally questionable, the direction of research has changed as to finding ways to lower the degree of fluorination or to replace them. Examples of surfactants which have been extensively investigated are partly fluorinated sulfosuccinate surfactants<sup>22-24</sup>, phosphate surfactants<sup>19, 25</sup> and numerous self-designed surfactants<sup>26, 27</sup>. A very interesting study was presented by Sagisaka *et al.* who systematically studied the influence of the tail length of various double-tail anionic surfactants on the properties of w/c-microemulsions. They found that the highest amount of water could

be solubilized using surfactants with a tail length of 12-14 Å<sup>28</sup>. Surfactants with different molecular structures possessing a low fluorine content have been investigated by Mohamed *et al.*, indicating that double-branched sodium sulfate surfactants are appropriate candidates for the formulation of microemulsions with supercritical CO<sub>2</sub><sup>29</sup>.

In this work we present an alternative method to improve the efficiency of fluorinated surfactants to formulate CO<sub>2</sub>-microemulsion and therewith reducing the required amounts of these environmentally questionable surfactants. We show that the addition of a low-molecular hydrophobic substance like cyclohexane can improve the efficiency of the microemulsion system brine – CO<sub>2</sub> – Zonyl FSO 100/ Zonyl FSN 100. Cyclohexane has been chosen for at least two reasons: first of all cyclohexane is known to be a penetrating oil<sup>30</sup>. Furthermore, having in mind to use SANS and film contrast conditions to elucidate the microstructure of these new type of CO<sub>2</sub>-microemulsions, cyclohexane turned out to be the preferred hydrophobic additive, because of the low price of the deuterated compound. In more detail we studied the influence of cyclohexane on the phase behavior at four different pressures between  $p = 150$  bar and  $p = 300$  bar. In order to investigate whether the unexpected increase of efficiency is induced by repulsive interactions between the hydrocarbon (cyclohexane) and the fluorinated surfactant tails a systematic small angle neutron scattering contrast variation study was performed. We will show that via the utilization of this technique the distribution of cyclohexane in a CO<sub>2</sub>/cyclohexane swollen micelle stabilized by fluorinated surfactants can be fully elucidated.

## B Experimental section

### I. Materials

The technical grade fluorinated surfactants are commercially available polyethyleneglycol-perfluoroalkylether of the type F-(CF<sub>2</sub>)<sub>*i*</sub>-(CH<sub>2</sub>CH<sub>2</sub>O)<sub>*j*</sub>-H (denoted as C<sub>*i*</sub>FE<sub>*j*</sub>) and were purchased from Sigma Adrich. Both the surfactants Zonyl FSN 100 ( $i = 6-8$ , degree of ethoxylation  $j = 8$  to 12) and Zonyl FSO 100 ( $i = 6-8$ , degree of ethoxylation  $j = 6$  to 10) were solved in ethanol, dried over NaSO<sub>4</sub> to remove water, filtered and ethanol was removed using a rotating evaporator prior to use. NaCl (purity > 99.5%) was purchased from Fluka (Neu Ulm, Germany), and D<sub>2</sub>O and cyclohexane-d<sub>12</sub> from Eurisotop (quoted > 99.9%). Water (H<sub>2</sub>O) was deionized and distilled twice. CO<sub>2</sub> (technically pure) was obtained from Linde AG (Munich, Germany) and cyclohexane-h<sub>12</sub> was provided by Sigma Aldrich with a purity > 99%. With the exception of the surfactants, all other materials were used without any further purification.

### II. Phase behavior

All phase behavior measurements under high pressure were performed using an in-house built high pressure view cell with variable volume. Thereby the transparent sapphire ring cylinder ( $h = 50$  mm,  $\varnothing_{\text{inside}} = 10$  mm,  $\varnothing_{\text{outside}} = 40$  mm) allows for a visual inspection of the sample<sup>10</sup>. The sample volume and thus the pressure can be adjusted with a tunable piston. The pressure is measured by a pressure transducer (Type 81530, Burster, Germany), which is inserted into the bottom of the view cell, with an accuracy of  $\pm 5$  bar. The maximum sample volume is 3.54 mL.

All samples were prepared directly inside the view cell. The amount of brine, surfactants and cyclohexane was controlled by weight with an accuracy of  $\pm 0.001$  g. A magnetic stir bar was added for homogenization. After sealing the cell with the piston liquid CO<sub>2</sub> was added to the cell using an in-house built filling apparatus

equipped with a membrane reservoir. The amount of CO<sub>2</sub> was calculated from the volume and the density of CO<sub>2</sub> under the given conditions. In order to study the phase behavior as function of temperature the view cell was placed in a water bath with temperature control of  $\pm 0.05$  K. When temperature equilibrium was reached the pressure was adjusted under magnetic stirring. The stirrer was turned off for the evaluation of the type and number of coexisting phases which was performed by visual inspection of both the transmitted and the scattered light. Subsequently this procedure was repeated at different temperatures and/or pressures until all phase boundaries were determined for the adjusted composition. The accuracy of the phase boundaries amounts to  $\pm 0.1^\circ\text{K}$  and  $\pm 10^\circ\text{bar}$ .

Two different kinds of sections through the phase prisms were performed at constant pressure to study the influence of cyclohexane on the phase behavior of CO<sub>2</sub>-microemulsion systems. A  $T(\gamma)$ -section through the upright Gibbs phase prism<sup>31-33</sup> has proven useful to characterize the general behavior of a ternary or pseudo-ternary microemulsion system. In such a section, the phase boundaries are recorded as a function of temperature and surfactant mass fraction

$$\gamma = \frac{m_{\text{surfactant}}}{\sum m_i} \quad (1)$$

at a constant ratio  $\alpha$  ( $\alpha = m_{\text{CO}_2}/(m_{\text{CO}_2} + m_{\text{brine}})$ ) of the two immiscible solvents. The general shape of the phase boundaries is shown in Fig.1 left by means of the system brine - CO<sub>2</sub> - non-ionic surfactant. At intermediate values of  $\gamma$ , an extended three phase region (3) can be found at ambient temperatures. Here, a microemulsion phase coexists with brine and CO<sub>2</sub> excess phases. The three-phase region meets the one-phase region at the so-called optimum point  $\bar{X}$ , which is given by the phase inversion temperature  $\bar{T}$  and the lowest surfactant mass fraction  $\bar{\gamma}$  needed to formulate a one-phase microemulsion. Note, that  $\bar{\gamma}$  is a measure of the efficiency of a surfactant to solubilize the two immiscible solvents.

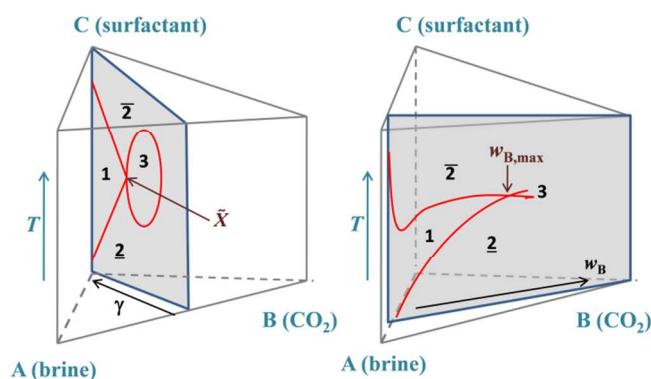


**Fig.1:**  $T(\gamma)$ -section (left) and  $T(w_B)$ -section (right) through the upright phase prism at constant pressure. The  $T(\gamma)$ -section, which is often used for the characterization of an unknown microemulsion system, shows the phase boundaries as a function of temperature and surfactant mass fraction  $\gamma$ , keeping the brine-to-CO<sub>2</sub> ratio constant. The  $T(w_B)$ -section is applied for the formulation of water-rich c/w-microemulsions. Here, the phase boundaries are recorded as a function of temperature and oil mass fraction  $w_B$  at a constant surfactant-to-brine ratio.

Examining the phase behavior as a function of temperature a phase sequence can be observed which is analogous to that of non-ionic microemulsion systems containing liquid oils<sup>15</sup>. At low temperatures

a two phase coexistence (2) of a CO<sub>2</sub>-in-water (c/w)-microemulsion with a CO<sub>2</sub> excess phase is found, while at high temperatures a coexistence of a water-in-CO<sub>2</sub> microemulsion with a water-excess phase (2) occurs.

In contrast to the  $T(\gamma)$ -section,  $T(w_B)$ -sections are used in case water-rich c/w-microemulsions have to be formulated. Starting from the pseudo-binary brine – nonionic surfactant system the phase boundaries are recorded as a function of temperature and mass fraction of CO<sub>2</sub>

$$w_B = \frac{m_{\text{CO}_2}}{\sum m_i} \quad (2)$$

Thereby, the mass fraction  $\gamma_a$  of surfactant in the brine-surfactant mixture is kept constant. As can be seen in Fig.1 right the  $T(w_B)$ -section is dominated by a funnel shaped one-phase region limited by the (lower, 2→1) emulsification failure boundary (*efb*) and the (upper, 1→2) near critical boundary (*ncb*). The intersection of *efb* and *ncb* determines the maximum amount of CO<sub>2</sub> ( $w_{B,\text{max}}$ ) that can be solubilized in the brine-surfactant mixture. At higher values of  $w_B$  the three-phase region exists. Note, that also the phase behavior of water-rich c/w-microemulsions is analogous to that of well-known oil-in-water(o/w)-microemulsions<sup>14, 34</sup>.

Note, that in major parts of this study, CO<sub>2</sub> is partly replaced by cyclohexane. In this case the mixture of CO<sub>2</sub> and cyclohexane is considered to be one hydrophobic pseudo-component. Accordingly, the mass fraction of the CO<sub>2</sub>/cyclohexane mixture  $w_B$  in the sample is given by

$$w_B = \frac{m_{\text{CO}_2} + m_{\text{cyclohexane}}}{\sum m_i} \quad (3)$$

Thereby the composition of the CO<sub>2</sub>/cyclohexane mixture is specified by mass fraction

$$\beta = \frac{m_{\text{cyclohexane}}}{m_{\text{CO}_2} + m_{\text{cyclohexane}}} \quad (4)$$

Because a considerable amount of CO<sub>2</sub> is dissolved monomerically in water, we recognized that the mass fraction  $\beta_i$  of cyclohexane in the mixture of the CO<sub>2</sub><sub>*i*</sub>/cyclohexane solubilized inside the micelle/microemulsion domains is the more relevant parameter. It is given by

$$\beta_i = \frac{m_{\text{cyclohexane}}}{m_{\text{CO}_2,i} + m_{\text{cyclohexane}}} \quad (5)$$

where the mass  $m_{\text{CO}_2,i}$  of CO<sub>2</sub> inside the micelle or domain was calculated taking into account that 4 wt% of CO<sub>2</sub> are monomerically dissolved in water<sup>35</sup>. Note, that the trend of the CO<sub>2</sub> solubility in water with pressure and temperature was neglected, so that the phase boundaries and structures of one sample composition can be compared within the selected range of pressure and temperature.

### III. SANS-measurements

All contrast variation SANS-measurements were performed at the D11 instrument at the Institut Laue-Langevin in Grenoble, France. The two chosen detector distances 1.75 m and 10 m were combined with a collimation length of 8 m and 10.5 m, respectively. The wavelength for all samples was  $\lambda = 6 \text{ \AA}$ . Thus, the scattering vector  $q = 4\pi\sin(\theta/2)/\lambda$  ranged from 0.007 to  $0.35 \text{ \AA}^{-1}$ , where  $\theta$  is the scattering angle. The ILL specified a wavelength distribution of  $\Delta\lambda/\lambda = 0.09$  (full width at half maximum) for the D11 instrument.

The scattering of the samples were studied using a high pressure cell with variable volume (HP-SANS-cell). This stainless-steel cell is equipped with two large sapphire windows (thickness 12 mm, neutron path way 2 mm) for observing the phase behavior of the samples prior and after the SANS-measurement. The volume and thus the pressure of this cell can be controlled by a tunable piston. The pressure is measured by a pressure probe which is inserted into the bottom of the cell, allowing for pressures up to  $p = 300$  with an accuracy of  $\pm 5$  bar. The temperature of the HP-SANS cell can be varied between 10° and 70°C with an accuracy of  $\Delta T = \pm 0.1$  K by connecting a thermostat to the cell. The sample volume can be adjusted between 15 and 19 mL.

All samples were prepared directly into the HP-SANS-cell. A stock solution of brine and surfactant was weighted into the cell, followed by cyclohexane. The amount of liquid CO<sub>2</sub> was adjusted by the position of the tunable piston, which was accurately determined using a dial gauge. Having added a magnetic stir bar the sample can be homogenized, especially because it is possible to turn the cell head over using a special holding. Before the SANS measurements the phase behavior is rechecked using the procedure described in section B II. Afterwards the sample holder was placed directly onto the sample mount of the D11 spectrometer.

The scattered neutrons were detected using a quadratic and two-dimensional <sup>3</sup>He multi-detector with 128 x 128 detector pixels with a size of 7.5 x 7.5 mm. A beam stop was positioned in front of the detector to prevent damage of the detector. The area around the beam stop was discarded from the scattering spectrum through masking. The normalization of the scattering intensity to the absolute scale was performed using the incoherent scattering of H<sub>2</sub>O as reference. The raw data treatment, masking and radial averaging to obtain a one dimensional scattering spectrum was performed using the standard evaluation software LAMP which is provided by the ILL and also accounts for the dead time of the detector. All measurements were background corrected. Although a few data points from the highest and lowest  $q$ -values were discarded from some measurements, the datasets from different sample-to-detector distances overlapped without adjustment.

### C Scattering Theory

There are basically two different approaches to obtain structural information out of scattering data which both should lead to the same results. The first one is to compare the measured scattering intensities to calculated scattering curves of a given structural model, which directly leads to numerical parameters such as particle size and size distribution. However, this approach has to be done carefully. Thus, one has to ensure that no models with too many adjustable or unknown parameters are used. In the ideal case, the shape of the structure is determined by a complementary method prior to the data analysis.

The second approach is to Fourier transform the scattering data to real space, which results in the pair distance distribution function (PDDF)  $p(r)$ . By evaluation of the shape and maximum extension of the PDDF information on the particle size and shape can be gained, meaning that this method can also be used if the shape of the structure is unknown. Here, the number of parameters is very restricted, but this route is also theoretically more demanding. Furthermore, in case of non-diluted interacting systems a structure factor has to be provided for the analysis of the data which hence is not model-free.

## I. Scattering models for microemulsion droplets

SANS experiments provide the scattering intensity  $I(q)$  in reciprocal space, i.e. as a function of scattering vector  $q$ . To gain information on the real-space structure, the scattering intensity of  $N$  particles in a volume  $V$  can be factorized into inter- and intraparticle scattering contributions (decoupling approximation<sup>36</sup>)

$$I(q) = n \cdot P(q) \cdot S(q) \quad (6)$$

with

$$n = \phi_{c,i} \frac{a_c}{4\pi v_c (R_0^2 + \sigma^2)} \quad (7)$$

being the particle number density of polydisperse spheres  $N/V$ . The form factor  $P(q)$  describes the intraparticle scattering and is related to the shape of the particles. The structure factor  $S(q)$  accounts for scattering contributions arising from the interference of neutrons scattered from different particles.

The form factor is defined as the product of the squared scattering length density difference  $\Delta\rho$ , the squared particle volume  $V_{\text{part}}$  and the complex square of the normalized scattering amplitude  $A(q)$  according to

$$P(q) = \Delta\rho^2 \cdot V_{\text{part}}^2 \cdot A(q) \cdot A^*(q). \quad (8)$$

The scattering amplitude  $A(q)$  is the Fourier transform of the scattering length density profile  $\Delta\rho(r) = \Delta\rho f(r,R)$  with  $\Delta\rho$  being the scattering contrast and  $f(r,R)$  the radial density distribution function that describes the density profile of the scattering particle. The polydispersity of droplet microemulsions is taken into account by the convolution of the droplet form factor  $P(q,R)$  with a Gaussian distribution function  $W(R,R_0,\sigma)$

$$W(R,R_0) = \frac{1}{\sqrt{2\pi\sigma^2}} \exp\left\{-\frac{(R-R_0)^2}{2\sigma^2}\right\}. \quad (9)$$

Here,  $R_0$  is the mean radius and  $\sigma$  the standard deviation of the droplet size distribution. Note, that for a sufficiently low  $\sigma$  polydispersity effects are independent of the type of the chosen size distribution<sup>37</sup>.

It was found that in most cases the interparticle interactions of microemulsion droplets formulated with non-ionic surfactants can be described by a repulsive hard-sphere potential<sup>38, 39</sup>. Hence, for a monodisperse system the Percus-Yevick structure factor for hard spheres can be used in order to describe interparticle scattering contributions<sup>40, 41</sup>. Since interparticle interactions are also affected by the polydispersity a Gaussian size distribution  $W(R_{\text{HS}}, R_{\text{HS},0}, \sigma_{\text{HS}})$  of the hard-sphere radius  $R_{\text{HS}}$  around its mean value  $R_{\text{HS},0}$  is convoluted with the Percus-Yevick structure factor. This averaged structure factor, in the following simply denoted as  $S_{\text{PY}}(q)$ , represents a weighted addition of monodisperse structure factors. The free fitting parameters are the hard-sphere interaction radius  $R_{\text{HS}}$ , its standard variation  $\sigma_{\text{HS}}$  and the hard-sphere volume fraction  $\phi_{\text{disp}}$ .

In case of water-rich microemulsions a hydrophobic substance, here a  $\text{CO}_2$ /cyclohexane-mixture (core) is separated by an amphiphilic film from water (bulk). Performing neutron scattering experiments on this type of systems the contrast is given by three scattering length densities  $\rho_{\text{core}}$ ,  $\rho_{\text{film}}$  and  $\rho_{\text{bulk}}$ . The so-called film contrast turned out to be an appropriate contrast to study the microstructure of w/o- as well as w/o-

microemulsions<sup>42-44</sup>. Here, where  $\rho_{\text{core}} = \rho_{\text{bulk}} \neq \rho_{\text{film}}$ , only the amphiphilic film contributes to the scattering intensity. However, often the exact composition of core, bulk and film are unknown leading to scattering contributions of both the amphiphilic film and the core of the micelle, i.e.  $\rho_{\text{core}} \neq \rho_{\text{bulk}} \neq \rho_{\text{film}}$ <sup>45</sup>. One model that accounts for both film and core scattering contributions of e.g. microemulsion droplets was developed by Foster<sup>46</sup>. He suggested a radial density distribution function defined as

$$f_{\text{droplet}}(r,R) = \frac{1}{\exp\left(\frac{r-R-\frac{d}{2}}{\chi}\right) + 1} - \frac{1 - \Delta\rho_{\text{core}}/\Delta\rho_{\text{film}}}{\exp\left(\frac{r-R+\frac{d}{2}}{\chi}\right) + 1} \quad (10)$$

where  $\Delta\rho_{\text{core}} = \rho_{\text{bulk}} - \rho_{\text{core}}$  and  $\Delta\rho_{\text{film}} = \rho_{\text{bulk}} - \rho_{\text{film}}$ ,  $R$  is the mean radius of the droplet and  $d$  is the shell thickness. The parameter  $\chi$  defines the shape of the resulting profile that can be step-like ( $\chi \rightarrow 0$ ), Gaussian-like, hyperbolic or parabolic. Using this distribution function the scattering length density profile of the droplet is given by  $\Delta\rho_{\text{droplet}}(r) = \Delta\rho_{\text{film}} f_{\text{droplet}}(r,R)$ .  $P_{\text{droplet}}(q)$  is obtained by Fourier transformation of  $\Delta\rho_{\text{droplet}}(r)$

$$P_{\text{droplet}}(q) = \Delta\rho^2 V_{\text{part}}^2 \left[ 4\pi \int_0^\infty \Delta\rho_{\text{droplet}}(r) \cdot r^2 \cdot \frac{\sin(qr)}{qr} dr \right]^2. \quad (11)$$

In order to describe the scattering intensity over the entire  $q$ -range the convoluted form factor (Eq(11)) is multiplied with the structure factor  $S_{\text{PY}}(q)$ . Note, that because the form factor cannot be calculated analytically MATHEMATICA 7.0<sup>TM</sup> was used to calculate it numerically.

## II. Generalized Indirect Fourier Transformation

For a model-free analysis of the scattering curves, the recorded scattering data are transformed to real space using the inverse Fourier transform<sup>47</sup>

$$p(r) = \frac{1}{2\pi^2} \int_0^\infty I(q)(qr) \sin(qr) dq \quad (12)$$

which yields the pair distance distribution function (PDDF)  $p(r)$ . However, applying the direct Fourier transformation requires scattering data of the full  $q$ -range, i.e.  $0 \leq q \leq \infty$ . The limited  $q$ -range available in small angle scattering experiments would lead to strong oscillations (termination effects) in such a direct Fourier transformation. These oscillations can be minimized using the indirect Fourier transformation (IFT)<sup>48, 49</sup> where a limitation of the PDDF is assumed and the PDDF is smoothed, desmeared and Fourier transformed in a simultaneous process. However, this method is restricted to samples which are highly diluted, i.e. it is assumed that no interparticle interactions occur ( $S(q) = 1$ ). Also based on the general idea that the PDDF and hence its Fourier transform can be described by a finite number of base functions, Glatter *et al.* developed a more general way

to analyze scattering data with interparticle interactions. This method is called the *Generalized Indirect Fourier Transformation* (GIFT)<sup>50, 51</sup>. Using the GIFT method, it is also possible to determine the particle form factor  $P(q)$  with a minimum of a priori information. The structure factor is calculated by separating its scattering contribution from the form factor scattering by means of factorization (see Eq(6)) and hence is not model-free. In this work the polydisperse Percus-Yevick structure factor was applied for all calculations using the GIFT procedure. The form factor and the structure factor are approximated in an iterative procedure by means of a nonlinear least-square procedure based on a Boltzmann-Simplex-Simulated-Annealing (BSSA) algorithm<sup>51</sup>. All in all the *a priori* information which is needed is an upper limit of the particle size for the form factor and a range for the volume of the scattering particle  $\phi_{\text{disp}}$ , the radius of the hard-sphere particle  $R_{\text{HS}}$  and its polydispersity  $\sigma_{\text{HS}}$  for the structure factor. The assumption that the PDDF can be described by a finite number of base functions can also be applied to a subsequent numerical deconvolution of the PDDF to obtain the radial scattering length density profile of the particle. This procedure is implemented into the DECON-tool of the GIFT program package developed by Glatter and Mittelbach<sup>52, 53</sup>. This program only needs information on the size distribution function assumed for the particles. Both the GIFT procedure and the DECON tool have already been applied to microemulsions under normal pressure<sup>54</sup> as well as under high pressure<sup>34</sup>.

## D Results and Discussion

### I. Phase behavior

In order to characterize the influence of cyclohexane on the phase behavior of CO<sub>2</sub>-microemulsions a series of  $T(\gamma)$  sections through the phase prism (see Fig.1) were performed at four different pressures at a constant mass fraction  $\alpha = 0.40$  of CO<sub>2</sub>/cyclohexane in the mixture of brine and CO<sub>2</sub>/cyclohexane. Such a  $T(\gamma)$  section through the phase prism is shown in Fig.2, left for the system brine –

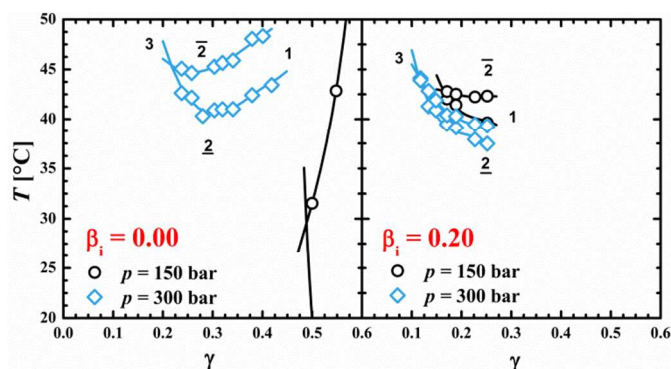


**Fig.2:**  $T(\gamma)$ -section of the systems brine – CO<sub>2</sub>/cyclohexane – Zonyl FSO 100/ Zonyl FSN 100 with  $\alpha = 0.40$ ,  $\delta_{\text{FSN}} = 0.75$  and  $\epsilon = 0.01$  shown at  $p = 150$  bar and  $p = 300$  bar. Left: System without cyclohexane, i.e.  $\beta_i = 0.00$ . Right: System containing 20 wt% of cyclohexane in the microemulsion domains swollen by the CO<sub>2</sub>/cyclohexane mixture, i.e.  $\beta_i = 0.20$ . Without cyclohexane a large mass fraction  $\tilde{\gamma}$  of surfactant is needed to solubilize brine and scCO<sub>2</sub>, especially at  $p = 150$  bar. Upon the partial replacement of scCO<sub>2</sub> with cyclohexane the solubilization efficiency of the surfactant mixture increases considerably for both pressures.

CO<sub>2</sub> – Zonyl FSO 100/ Zonyl FSN 100 at  $\delta_{\text{FSN}} = 0.75$ . A brine solution containing 1 wt% NaCl ( $\epsilon = 0.01$ ) was used in order to screen electrostatic interactions caused by ionic impurities. As mentioned already in Section B II for all studied pressures ( $p = 200$  bar and  $p = 250$  bar are not shown) a temperature dependent phase sequence can be found which is analogous to that of non-ionic microemulsion systems containing liquid oils<sup>34, 55</sup>. In the left figure (cyclohexane-free system) the strong effect of the pressure on the phase behavior becomes obvious. The mass fraction of surfactant  $\tilde{\gamma}$  needed to solubilize brine and scCO<sub>2</sub> decreases from  $\tilde{\gamma} = 0.50$  to  $\tilde{\gamma} = 0.22$  by increasing the pressure from  $p = 150$  bar to  $p = 300$  bar. This pressure-induced increase in efficiency can be ascribed to the better interaction between the surfactant and CO<sub>2</sub>-molecules caused by an increase in CO<sub>2</sub> density<sup>34</sup>. Furthermore, the shape of the phase boundaries recorded at  $p = 300$  bar are typical for microemulsions with efficient technical grade surfactants<sup>56</sup>. The distortion of the phase boundaries at low  $\gamma$ -values towards higher temperatures can be explained by the distribution of the ethoxylation degree and a residual amount of non-reacted alcohol (the chain length of the alcohol is rather narrow distributed). Especially, the hydrophobic non-reacted alcohol and the surfactant species with lower degree of ethoxylation are dissolved monomerically in CO<sub>2</sub>. Decreasing the surfactant mass fraction  $\gamma$  by adding brine and CO<sub>2</sub> one extracts increasing amounts of the more hydrophobic fractions of the surfactant mixture from the amphiphilic film, which accordingly becomes increasingly hydrophilic. Following the properties of ternary non-ionic microemulsions the phase behavior shifts to higher temperatures with decreasing  $\gamma$ , explaining the large distortion of the phase boundaries. The phase behavior of the system in which 20 wt% of CO<sub>2</sub> in the respective microemulsions domains is replaced with cyclohexane, i.e.  $\beta_i = 0.20$  is shown in Fig.2 right. As can be seen, the partial replacement leads to a strong unexpected shift of the phase boundaries towards lower surfactant mass fractions. At  $p = 300$  bar, the mass fraction of surfactant  $\tilde{\gamma}$  at the optimum point  $\tilde{X}$  decreases from  $\tilde{\gamma} = 0.22$  for the cyclohexane-free system to  $\tilde{\gamma} = 0.11$  for the cyclohexane-containing system. More impressively even is the cyclohexane induced change of phase behavior at 150 bar, as  $\tilde{\gamma}$

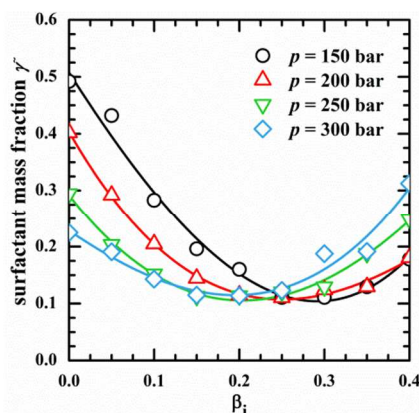


**Fig.3:** Plot of the optimum surfactant mass fraction  $\tilde{\gamma}$  as a function of the mass fraction  $\beta_i$  of cyclohexane in the CO<sub>2</sub>/cyclohexane domains determined for the system brine – CO<sub>2</sub>/cyclohexane – Zonyl FSO 100/Zonyl FSN 100 at  $\alpha = 0.40$ ,  $\delta_{\text{FSN}} = 0.75$  and  $\epsilon = 0.01$ . For the four pressures studied  $\tilde{\gamma}$  runs through a pronounced minimum. While the position of the minimum shifts to larger values of  $\beta_i$  with decreasing pressure, all curves reach nearly the same minimum value of  $\tilde{\gamma}_{\text{min}} = 0.11 \pm 0.01$ . Note, that  $\tilde{\gamma}$  was determined with a precision of  $\pm 0.01$ .

decreases from  $\tilde{\gamma} = 0.50$  to  $\tilde{\gamma} = 0.16$ . Furthermore, the distortion of the phase boundaries at low  $\gamma$ -values caused by the extraction of the hydrophobic surfactant species from the interface becomes more pronounced.

This unexpected cyclohexane-induced increase of efficiency was systematically characterized recording a series of additional  $T(\gamma)$  sections at cyclohexane mass fractions of  $\beta_i = 0.05, 0.10, 0.15$  and  $0.25$ . In Fig.3 the values obtained for the surfactant mass fraction  $\tilde{\gamma}$  at the optimum point are plotted as a function of  $\beta_i$  for  $p = 150, 200, 250$  and  $300$  bar.

With increasing amount of cyclohexane in the  $\text{CO}_2$ /cyclohexane domains the mass fraction  $\tilde{\gamma}$  of fluorinated surfactant needed to formulate a  $\text{CO}_2$ -microemulsion runs through an pronounced minimum, which is located at  $\tilde{\gamma}_{\min} = 0.11 \pm 0.01$  regardless of the adjusted pressure. Thereby the position of the minimum increases with decreasing pressure from  $\beta_i = 0.19$  at  $p = 300$  bar to  $\beta_i = 0.29$  at  $p = 150$  bar. Note, that the full lines drawn to guide the eye are polynomial functions of third order.

In order to understand this considerable and unexpected efficiency boosting effect induced by cyclohexane one may consider the interactions between the  $\text{CO}_2$ /cyclohexane mixture and the fluorinated alkyl chain of the surfactants. Repulsive interactions between fluorinated surfactants and hydrogenated substances like cyclohexane are known to be present<sup>57, 58</sup>. These repulsive interactions are likely to reduce the monomeric solubility of the fluorinated surfactants in the  $\text{CO}_2$ /cyclohexane mixture, which is rather high (11 wt%) in case pure  $\text{CO}_2$  is solubilized<sup>34</sup>. A lower monomeric solubility means that more surfactant is available at the interface, which would result in a higher efficiency.

However, the decreasing monomeric solubility is by far from being sufficient to explain the enormous efficiency increase especially at 150 bar. The majority of this effect might be explained by another consequence of the repulsive interactions between cyclohexane and the fluorinated alkyl chain of the surfactant. As the interactions between  $\text{CO}_2$  and the fluorinated surfactants are far more attractive than the ones between cyclohexane and the surfactants, it is likely that a concentration gradient of cyclohexane within the respective microemulsion domains develops. Thus, we propose the formation of a depletion zone of cyclohexane close to the surfactants and a cyclohexane-enriched zone at the center of the domains, where the repulsive interactions are diminished. In this context, the observed trend of  $\tilde{\gamma}$  with  $\beta_i$  might be discussed as follows: Increasing the mass fraction  $\beta_i$  of cyclohexane in the  $\text{CO}_2$ -swollen domains leads to the formation of a depletion zone, which becomes more and more pronounced and causes a considerable decrease of  $\tilde{\gamma}$ , i.e. an increase of efficiency. Above a certain (pressure dependent) concentration of cyclohexane, the cyclohexane molecules cannot avoid the repulsive interactions causing a decrease of efficiency.

In order to prove this hypothesis, i.e. whether a depletion zone of cyclohexane is formed near the amphiphilic surfactant film we performed Small Angle Neutron Scattering (SANS) experiments, applying a systematic contrast variation. Using the *Generalized Indirect Fourier Transformation* (GIFT) procedure it is possible to extract the scattering length density distribution which reveals the distribution of  $\text{CO}_2$  and cyclohexane in the microemulsion domains. As the GIFT procedure has proven to be in particular applicable to dilute microemulsions systems where the interparticle interactions are known and thus can be considered by the appropriate structure factor, we decided to

prove the hypothesis by means of water-rich c/w-microemulsions.

As described in Section B II the phase behavior of water-rich microemulsion is best-investigated recording  $T(w_B)$  sections through the phase prism (see Fig.1 right). The phase behavior of the system under study, i.e. the system brine –  $\text{CO}_2$ /cyclohexane – Zonyl FSO 100/ Zonyl FSN 100 is shown in Fig.4 at a constant mass fraction  $\gamma_a = 0.08$  of the surfactant mixture ( $\delta_{\text{FSN}} = 0.75$ ) in the brine/surfactant mixture.

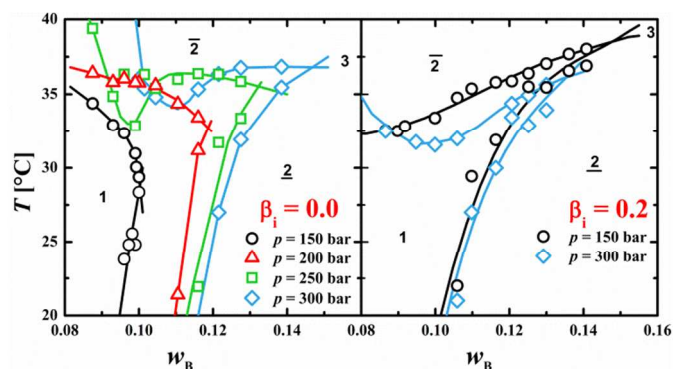


**Fig.4:**  $T(w_B)$ -sections of the system brine –  $\text{CO}_2$ /cyclohexane – Zonyl FSO 100/ Zonyl FSN 100 at  $\gamma_a = 0.08$ ,  $\delta_{\text{FSN}} = 0.75$  and  $\varepsilon = 0.01$  shown at different pressures. Left: System without cyclohexane, i.e.  $\beta_i = 0.00$ . The ability to solubilize  $\text{CO}_2$  increases considerably with pressure. Right: System containing 20 wt% of cyclohexane in the micelles swollen by the  $\text{CO}_2$ /cyclohexane mixture, i.e.  $\beta_i = 0.20$ . Upon the partial replacement of  $\text{CO}_2$  with cyclohexane, the solubilization capacity increases considerably at  $p = 150$  bar, i.e. almost the same amount of  $\text{CO}_2$  can be solubilized at  $p = 150$  and  $p = 300$  bar.

As can be seen, also in the water-rich regime of the phase prism the shape of the phase boundaries is analogous to that of non-ionic microemulsion systems containing liquid oils<sup>32, 59-61</sup>. On the left-hand side in Fig.4 the  $T(w_B)$ -sections of the system without cyclohexane ( $\beta_i = 0.00$ ) are shown. They illustrate that the phase behavior is strongly affected by pressure, i.e. with increasing pressure the maximum amount  $w_{B,\max}$  of  $\text{CO}_2$  that can be solubilized is considerably increased. The emergence of a minimum in the upper near critical phase boundary which is equivalent to the formation of a so-called loop at  $p = 250$  bar and  $300$  bar indicates that the microemulsion undergoes a change from weakly (no loop) to strongly (pronounced loop) structured<sup>62</sup> with increasing pressure. Upon the partial replacement of  $\text{CO}_2$  with cyclohexane ( $\beta_i = 0.20$ ) the general phase sequence remains the same (shown on the right hand side of Fig.4). However, the maximum amount of  $\text{CO}_2$  and cyclohexane which can be solubilized by the surfactant mixture increases, especially at  $p = 150$  bar. Here almost the same amount of  $\text{CO}_2$  and cyclohexane can be solubilized at  $p = 150$  and  $p = 300$  bar.

## II. Small Angle Neutron Scattering – contrast variation

In order to investigate the distribution of cyclohexane in the  $\text{CO}_2$ -rich core of the micelles stabilized by the fluorinated surfactant mixture a systematic SANS contrast variation was performed in the system  $\text{H}_2\text{O}/\text{D}_2\text{O}/\text{NaCl} - \text{CO}_2$ /cyclohexane – Zonyl FSO 100/Zonyl FSN 100 at  $\gamma_a = 0.08$ ,  $\delta_{\text{FSN}} = 0.75$ ,  $\varepsilon = 0.01$ ,  $\beta_i = 0.20$ ,  $w_B = 0.10$  and  $T = 20^\circ\text{C}$ . In order to

determine the scattering length density of the technical-grade surfactant mixture we performed a contrast variation of the pseudo-binary system brine – Zonyl FSO 100/Zonyl FSN 100 at  $\delta_{\text{FSN}} = 0.75$  and  $\gamma_a = 0.08$ , beforehand. The scattering of samples with nine different ratios of H<sub>2</sub>O/D<sub>2</sub>O were recorded. In Fig.5 the scattering intensity (after subtracting of the incoherent scattering contribution  $I_{\text{incoh}}$ ) extrapolated towards  $q = 0 \text{ \AA}^{-1}$  was plotted as a function of the volume fraction of D<sub>2</sub>O in the H<sub>2</sub>O/D<sub>2</sub>O-mixture. As can be seen  $I(0) - I_{\text{incoh}}$  runs through a minimum at  $\phi_{\text{D}_2\text{O}} = 0.35$ , which means that the scattering length density of the surfactant mixture is  $1.84 \cdot 10^{10} \text{ cm}^{-2}$  which slightly lower than the results of Klostermann *et al.*<sup>34</sup>.

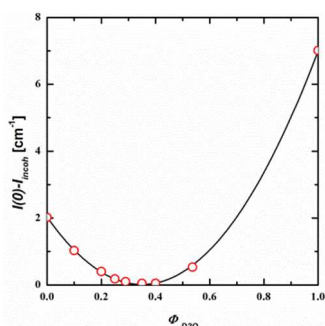


**Fig.5:** Scattering intensity of nine samples with different ratios of H<sub>2</sub>O/D<sub>2</sub>O (extrapolated towards  $q = 0 \text{ \AA}^{-1}$  and after subtraction of  $I_{\text{incoh}}$ ) as a function of the volume fraction of D<sub>2</sub>O in the H<sub>2</sub>O/D<sub>2</sub>O mixture. The data were obtained performing a contrast variation in the pseudo-binary system brine – Zonyl FSO 100/Zonyl FSN 100 at  $\delta_{\text{FSN}} = 0.75$ ,  $\gamma_a = 0.08$ ,  $\varepsilon = 0.01$  and  $T = 20^\circ\text{C}$  in order to determine the scattering length density of the technical grade fluorinated surfactant mixture. The minimum of the polynomial fit is located at  $\phi_{\text{D}_2\text{O}} = 0.35$ .

With this knowledge we adjusted four different contrasts which are shown schematically in Fig.6. The scattering length densities of the single components were calculated using the NIST scattering length density calculator<sup>63</sup>. In order to calculate the scattering length density of the core we assumed a homogeneous distribution of CO<sub>2</sub> and cyclohexane inside the swollen micelle (though it is in contradiction with our hypothesis). Furthermore, we took into account that 4 wt% of CO<sub>2</sub> is dissolved in brine and the monomeric solubility of the fluorinated surfactants in the CO<sub>2</sub>/cyclohexane mixture was set to 4 wt% (which is much lower than in the CO<sub>2</sub>-microemulsion without cyclohexane). Note, that the trends of both quantities with pressure and temperature were neglected.

At contrast condition A protonated cyclohexane-h12 (scattering length density of  $\rho_{\text{cyclohexane-h12}} = -0.28 \cdot 10^{10} \text{ cm}^{-2}$ ) was used in a mixture with CO<sub>2</sub>, which at 20°C and  $p = 150$  bar has a scattering length density of  $2.3 \cdot 10^{10} \text{ cm}^{-2}$ . Thus, the scattering length density of the CO<sub>2</sub>/cyclohexane-h12 mixture results to  $1.7 \cdot 10^{10} \text{ cm}^{-2}$ , which is very similar to the scattering length density of the surfactants. The scattering length density of the bulk was adjusted to  $3.1 \cdot 10^{10} \text{ cm}^{-2}$  using a volume fraction  $\phi_{\text{D}_2\text{O}} = 0.54$  of D<sub>2</sub>O in the H<sub>2</sub>O/D<sub>2</sub>O mixture. This means that in contrast A both the amphiphilic film as well as micellar core (CO<sub>2</sub>/cyclohexane) contribute to the scattering intensity.

In contrast to that, only core scattering contributions were obtained in contrast B by using deuterated ( $\rho_{\text{cyclohexane-d12}} = 6.7 \cdot 10^{10} \text{ cm}^{-2}$ ) instead of protonated cyclohexane. Thus, the scattering length density of the

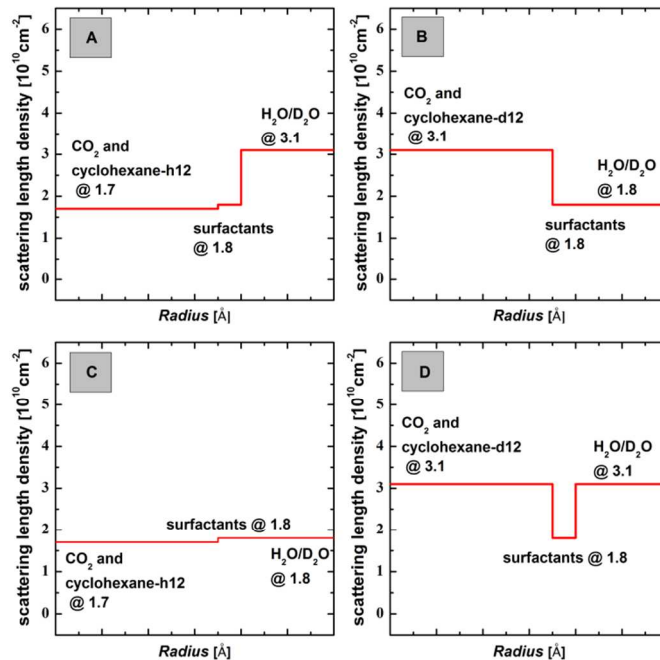


**Fig.6:** Schematic representation of the four different contrast conditions adjusted in this study, assuming a homogeneous distribution of CO<sub>2</sub> and cyclohexane inside the swollen micelle. In contrast A the overall micellar core (CO<sub>2</sub>/cyclohexane) as well as the amphiphilic film) contributes to the scattering intensity whereas at contrast B only the core provides scattering contributions. Contrast C was aimed to match all three scattering length densities. Film contrast condition was intended in contrast D. The scattering length densities were calculated at a temperature of  $T = 20^\circ\text{C}$  and  $p = 150$  bar.

CO<sub>2</sub>/cyclohexane-d12 mixture results to  $3.1 \cdot 10^{10} \text{ cm}^{-2}$  at 20°C and 150 bar. The scattering length density of the bulk was adjusted to match that of the surfactants by using a volume fraction of  $\phi_{\text{D}_2\text{O}} = 0.35$ . In order to assess the quality of the scattering length density calculations, contrast C was chosen to match all three scattering length densities. Therefore both the core and the bulk scattering length densities were adjusted to the one of the surfactants using protonated cyclohexane-h12 and  $\phi_{\text{D}_2\text{O}} = 0.35$ . In condition D we aimed for the so-called film contrast, in which only the amphiphilic surfactant film contributes to the scattering intensity. Using a CO<sub>2</sub>/cyclohexane-d12 mixture and  $\phi_{\text{D}_2\text{O}} = 0.54$  the scattering length density of core and bulk was adjusted to  $3.1 \cdot 10^{10} \text{ cm}^{-2}$ .

The recorded scattering curves together with the intensities calculated using the form factor  $P_{\text{droplet}}(q)$  of polydisperse spherical droplets (see Eq(11))<sup>34, 46</sup> and the polydisperse Percus-Yevick structure factor  $S_{\text{PY}}(q)$ <sup>40, 41</sup> are shown in Fig.7. Thereby, the incoherent scattering contribution  $I_{\text{incoh}}$  has been subtracted from the scattering curves recorded at  $p = 100, 150$  and 200 bar. As can be seen, the scattering curves obtained for the contrast A, B and C show the typical features found in spectra from polydisperse spherical droplets recorded in bulk contrast and in the limit of a comparatively low particle number density<sup>39, 64</sup>. Thus, the scattering curves indicate a constant scattering intensity at low  $q$ -values which changes over to a steep  $q^{-4}$ -dependence with increasing  $q$ . At  $q \approx \pi/R_0$  oscillations of the scattering intensity can be observed which are smeared by the droplet polydispersity  $\sigma$ .

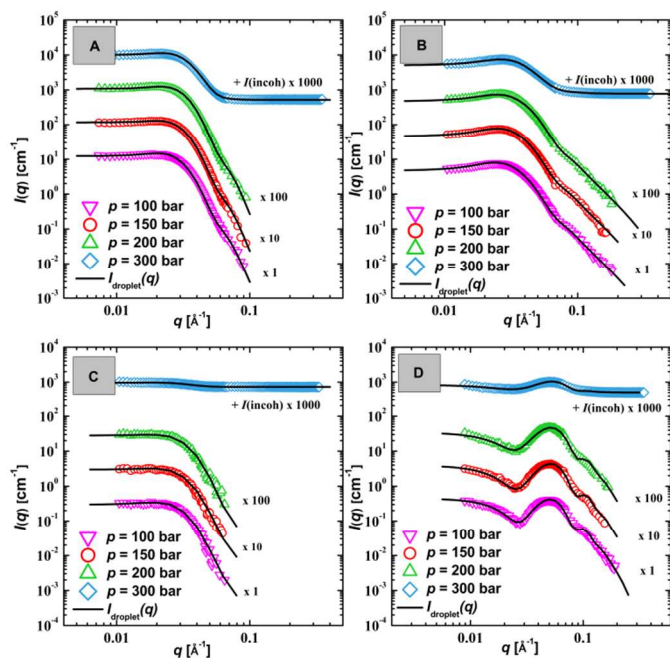


**Fig. 7:** Small angle neutron scattering curves of the sample brine – CO<sub>2</sub>/cyclohexane – Zonyl FSO 100/Zonyl FSN 100 at  $\gamma_a = 0.08$ ,  $\delta_{\text{FSN}} = 0.75$ ,  $\varepsilon = 0.01$ ,  $\beta_i = 0.2$ ,  $w_B = 0.10$  and  $T = 20^\circ\text{C}$ , different pressures and contrast conditions (schematically depicted in Fig. 6). Note, that the incoherent scattering contribution  $I_{\text{incoh}}$  has been subtracted from the scattering curves recorded at  $p = 100, 150$  and  $200$  bar. The full lines which describe the experimental scattering curves almost quantitatively (small but systematic deviations in contrast D) were calculated using the droplet form factor  $P_{\text{droplet}}(q)$ <sup>34, 46</sup> for polydisperse spheres, convoluted with the polydisperse Percus-Yevick structure factor  $S_{\text{PY}}(q)$ <sup>40, 41</sup>.

The scattering intensity  $I_0$  at  $q \rightarrow 0$  strongly depends on the scattering contrast. As in contrast A and B similar absolute values of  $|\Delta\rho_{\text{core}}|$  were adjusted, the forward scattering is also similar. However, it is by one order of magnitude lower for contrast C and D in which either the scattering contrast or the volume fraction which contributes to the scattering intensity is very low. Note, that for these two contrasts the  $q^{-4}$  (C)/ $q^{-2}$  (D) decay as well as the oscillation become only visible by a subtraction of  $I_{\text{incoh}}(q)$  from the scattering curves.

Taking a closer look at the scattering curves recorded in film contrast (D), it might at first sight seem surprising that the pronounced minimum shifts to lower  $q$ -values with increasing pressure. Such a shift is usually an indication for a structural growth which in the case of a compression is not reasonable. However, describing the scattering curves quantitatively (see below) it turned out that the optimum film contrast condition was not achieved. An additional scattering contribution from the core which increases with increasing pressure was found to be responsible for the not intuitive shift of the minimum. As expected the mean radius  $R_0$  of the swollen micelles decrease with increasing pressure (Table 2).

In all cases the form factor  $P_{\text{droplet}}(q)$  of polydisperse spherical droplets (see Eq(11)) and the polydisperse Percus-Yevick structure factor  $S_{\text{PY}}(q)$  describe the scattering intensity almost quantitatively. Small but systematic deviations can be observed for  $q \geq \pi/R_0$ , i.e. for  $q$ -values slightly larger than the position of the oscillation especially in contrast D. Compared to the experimental data, the oscillation seems to be too pronounced

**Table 1:** Parameters of the Percus-Yevick structure factor obtained from the analysis of the scattering data (Fig. 7) of the system brine – CO<sub>2</sub>/cyclohexane – Zonyl FSO 100/Zonyl FSN 100 at  $\gamma_a = 0.08$ ,  $\delta_{\text{FSN}} = 0.75$ ,  $\varepsilon = 0.01$ ,  $\beta_i = 0.2$ ,  $w_B = 0.10$ ,  $T = 20^\circ\text{C}$  and different pressures. The hard-sphere interaction radius  $R_{\text{HS}}$  decreases with increasing pressure due to the increasing density of CO<sub>2</sub>. Note, that the values of the parameters obtained for the different contrasts are very similar.

contrast	$p/\text{bar}$	$R_{\text{HS}}/\text{\AA}$	$\sigma_{\text{HS}}/R_{\text{HS}}$
A	100	81	0.35
A	150	79	0.32
A	200	77	0.32
A	300	75	0.32
B	100	83	0.32
B	150	79	0.32
B	200	77	0.32
B	300	75	0.28
C	100	83	0.32
C	150	79	0.32
C	200	77	0.28
C	300	75	0.32
D	100	83	0.32
D	150	79	0.32
D	200	77	0.32
D	300	75	0.32

indicating that the used radial density distribution function (see Eq(10)) is not able to describe the distribution of CO<sub>2</sub> and cyclohexane inside the micelle quantitatively. We will come back to this point in the next section.

As the sample composition and temperature was kept constant for the adjusted four contrasts, the structure of the CO<sub>2</sub>-microemulsion should not change. That this is indeed the case becomes obvious comparing the values obtained for the hard-sphere interaction radius  $R_{\text{HS}}$  and the polydispersity  $\sigma_{\text{HS}}/R_{\text{HS}}$  compiled in Table 1. As can be seen, the values of the parameters obtained for the different contrasts are very similar. Furthermore, as expected from the trend of the CO<sub>2</sub>-density, the hard-sphere interaction radius  $R_{\text{HS}}$  decreases with increasing pressure.

The structural parameter of the numerical droplet form factor  $P_{\text{droplet}}(R)$  obtained from the analysis of the scattering data (Fig. 7) are summarized in Table 2. For each contrast the mean radius  $R_0$  of the microemulsion droplet decreases from  $p = 100$  bar and  $300$  bar by  $8 \pm 1$  Å. Furthermore, the values obtained for the radius at the contrasts B and C (both core contrast) are  $6 \pm 1$  Å smaller than the ones at contrast A in which the amphiphilic also contributes to the scattering intensity (core + film). That this value is somewhat smaller than the length of the surfactant molecules is related to the penetration of CO<sub>2</sub> into the fluorinated surfactant chains and water molecules into the surfactant head groups.

The most reliable value for the shell thickness  $d$  is obtained from the analysis of the film scattering data, which provides a thickness of the amphiphilic film between  $12$  and  $13$  Å. The analysis of the scattering data from contrast A and C provides values of  $d$  close to zero. Such low values of  $d$  can be explained as follows: In the case of  $d \approx 0$  the neutrons cannot distinguish between the amphiphilic film and the core (contrast A) or the solvent (C). As a consequence a broad transition of the

scattering length density, indicated by high values of  $\chi$ , is obtained for the contrasts A and C. This effect becomes particularly obvious by taking a closer look at the parameter obtained for contrast A. At  $p = 100$  bar the thickness  $d = 0$  Å is connected to the fact that  $\Delta\rho_{\text{core}} > \Delta\rho_{\text{film}}$ . This means that, starting from the core of the micelle, the SLD increases continuously towards the scattering length density of the bulk. As a result of the penetration of solvent molecules into the amphiphilic film no discrete step is observed in the SLD profile. Instead a very diffuse scattering profile with a large value of  $\chi$  is found. Increasing the pressure to  $p = 300$  bar, however, the contrast situation changes to  $\Delta\rho_{\text{core}} < \Delta\rho_{\text{film}}$ . In this case the SLD of the core is higher than that of the amphiphilic film but lower than the one of the solvent, which results in a minimum of the SLD profile at the film. Here, the neutrons can distinguish between the film and the core/solvent, resulting in a large value of the shell thickness i.e.  $d = 12$  Å.

Note that the absolute value of the scattering contrast  $|\Delta\rho_{\text{core}}|$  is the same for the contrast conditions A and B at  $p = 100$  bar. However, as the scattering length density of the core (CO<sub>2</sub>/cyclohexane) increases with increasing pressure, a decrease of  $|\Delta\rho_{\text{core}}|$  is found in the case of contrast A, while it increases in contrast B. Thereby, the pressure induced change of the core scattering length density, i.e.  $|\Delta\rho_{\text{core}}(p = 100 \text{ bar}) - \Delta\rho_{\text{core}}(p = 300 \text{ bar})|$ , is the same for the contrasts A, B and D.

**Table 2:** Parameters (mean radius  $R_0$ , polydispersity  $\sigma/R_0$ , shell thickness  $d$  and shape of the radial density distribution function  $\chi$ ) of the droplet form factor (see Eq(11)) obtained from the analysis of the scattering data (Fig.7) of the system brine – CO<sub>2</sub>/cyclohexane – Zonyl FSO 100/Zonyl FSN 100 at  $\gamma_a = 0.08$ ,  $\delta_{\text{FSN}} = 0.75$ ,  $\varepsilon = 0.01$ ,  $\beta_i = 0.2$ ,  $w_B = 0.10$ ,  $T = 20^\circ\text{C}$  and different pressures. The adjusted contrasts are given by  $\Delta\rho_{\text{core}} = \rho_{\text{bulk}} - \rho_{\text{core}}$  and  $\Delta\rho_{\text{film}} = \rho_{\text{bulk}} - \rho_{\text{film}}$ .

	$p/$ bar	$R_0/$ Å	$\sigma/R_0$	$d/$ Å	$\chi/$ Å	$\Delta\rho_{\text{core}}/$ $10^{-6} \text{ Å}^{-2}$	$\Delta\rho_{\text{film}}/$ $10^{-6} \text{ Å}^{-2}$
A	100	68	0.20	0.0	11.0	1.47	1.27
A	150	67	0.20	1.0	10.0	1.36	1.27
A	200	64	0.20	8.0	9.0	1.29	1.27
A	300	59	0.18	12.0	8.0	1.20	1.27
B	100	62	0.23	10.8	1.5	-1.49	0.25
B	150	60	0.25	10.8	1.3	-1.59	0.25
B	200	57	0.25	10.7	1.0	-1.66	0.25
B	300	54	0.25	10.7	1.0	-1.75	0.25
C	100	61	0.25	1.0	10.0	0.23	0.02
C	150	60	0.25	3.0	9.0	0.24	0.02
C	200	57	0.25	3.0	9.0	0.24	0.02
C	300	54	0.25	2.0	9.0	0.27	0.02
D	100	65	0.14	12.5	3.8	-0.58	1.27
D	150	64	0.14	12.5	3.8	-0.67	1.27
D	200	63	0.14	12.7	3.5	-0.71	1.27
D	300	59	0.16	13.0	3.0	-0.84	1.27

### III. Generalized Indirect Fourier Transformation (GIFT)

In order to elucidate the distribution of cyclohexane and CO<sub>2</sub> within the micelle the GIFT method was applied to the scattering curves shown in Fig.7<sup>50</sup>. For this analysis the Percus-Yevick structure factor of polydisperse spheres as described in section C I. was used for taking into account interparticle

interactions. Thereby the parameters used for the GIFT procedure are in good agreement with the ones shown in Table 1. The normalized pair distance distribution functions (PDDF)  $p(r)$  which were obtained from the Generalized Indirect Fourier Transformation of the scattering data are shown in Fig.8. The PDDFs of each contrast were normalized to the peak maximum of the PDDF at  $p = 100$  bar, thus keeping the area under the PDDF at the right ratio.

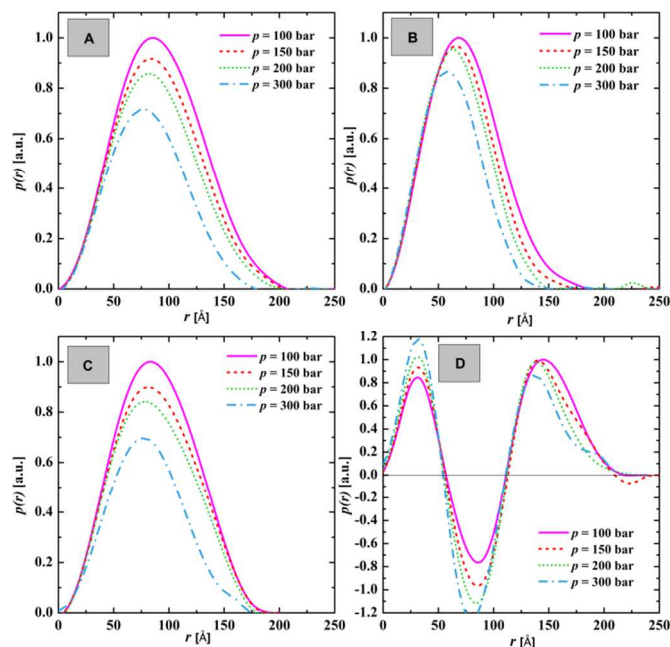


**Fig.8:** Pair distance distribution functions (PDDFs) of the scattering curves (see Fig.7) recorded for the microemulsion system brine – CO<sub>2</sub>/cyclohexane – Zonyl FSO 100/Zonyl FSN 100 at  $\gamma_a = 0.08$ ,  $\delta_{\text{FSN}} = 0.75$ ,  $\varepsilon = 0.01$ ,  $\beta_i = 0.2$ ,  $w_B = 0.10$ ,  $T = 20^\circ\text{C}$ , different pressures and contrast conditions (depicted in Fig.6). The PDDFs of the contrast A, B and C show the typical features of spherical structures, whereas the PDDF of contrast D resemble the features of inhomogeneous structures<sup>65</sup>.

The pair distance distribution functions of the contrasts A, B and C have a shape typical for polydisperse homogenous spheres<sup>66</sup>. Under the consideration of polydispersity effects the maximal extension of these PDDFs is in good agreement with the diameter of the droplets obtained from the fits of the scattering data. In order to interpret the PDDFs obtained for contrast condition D one has to be aware that the Pair Distance Distribution Function is a statistical function which represents the rate of occurrence of different distances between regions of the same scattering length density. Thus, the first maximum at about 30 Å represents small distances within the shell i.e. the amphiphilic film, and the second maximum at about 150 Å represents shell-shell distances. The minimum between the two maxima, however, has its origin in the fact that at least three different regions of SLD exist, i.e.  $\rho_{\text{core}} \neq \rho_{\text{bulk}} \neq \rho_{\text{film}}$ . By means of the DECON package it was possible to extract the scattering length density profiles out of the pair distance distribution functions. Note that these calculations were performed using the raw data from the GIFT procedure and not the normalized data shown in Fig.8. For a better overview only the profiles of  $p = 100$  and 300 bar are shown in Fig.9. The profiles which are deconvoluted from the PDDF are normalized to the volume of the scattering particle. Note, that in Fig.9 the

intrinsic scattering length density (not the one with respect to SLD of the bulk) is plotted. Therefore the SLD-profiles were shifted by the respective SLD-value of the bulk, i.e.  $3.1 \cdot 10^{10} \text{ cm}^{-2}$  for contrasts A and D and  $1.84 \cdot 10^{10} \text{ cm}^{-2}$  for contrasts B and C.

The most important thing to be noticed in Fig.9 is that all profiles exhibit a comparatively small homogeneous core and a wide transition range in which the SLD approaches the value of the bulk, respectively film in contrast D. Such a wide transition range differs substantially from previous results on similar  $\text{CO}_2$ -microemulsions without cyclohexane<sup>34</sup>. Klostermann *et al.* investigated microemulsions of the type brine –  $\text{CO}_2$ – Zonyl FSO 100/ Zonyl FSN 100 at very similar composition, temperature and pressure. For example, for a micelle with a mean radius of about  $R_0 \approx 115 \text{ \AA}$  they found that the scattering length density of the core remains constant for about  $95 \text{ \AA}$ , followed by a steep decrease of scattering length density difference within about  $20 \text{ \AA}$  onto the constant scattering length density of the bulk. For the cyclohexane containing

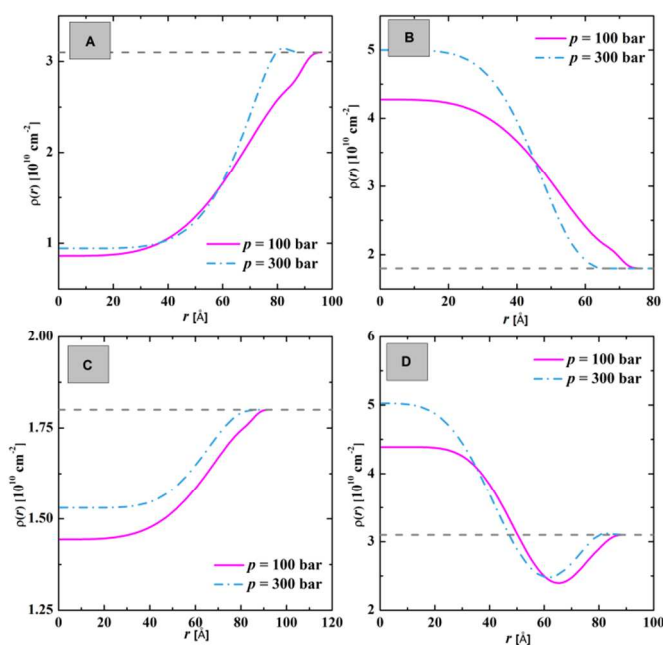


**Fig.9:** Radial scattering length density (SLD) profiles deconvoluted from the PDDFs (shown in Fig.8) for  $p = 100$  and  $300$  bar and the four adjusted contrast conditions. The profiles obtained for the contrasts A, B and C exhibit a homogeneous core and a wide transition range in which the SLD approaches the value of the bulk. The wide transition range is a strong indication of an inhomogeneous distribution of cyclohexane within the micelle, i.e. the formation of a depletion zone of cyclohexane close to the fluorinated amphiphilic film. Contrast D shows a minimum of the SLD between  $60$  and  $70 \text{ \AA}$ , which stems from the amphiphilic surfactant film. Furthermore, the SLD of the core is considerably larger than the SLD of the bulk which is another indication of an inhomogeneous distribution of cyclohexane within the micelle.

$\text{CO}_2$ -microemulsions studied here, in contrast, the scattering length density remains constant only for about  $45 \text{ \AA}$ , followed by a  $40 \text{ \AA}$  - wide increase until at about  $90 \text{ \AA}$  the scattering length density of the bulk material is reached (contrast A,  $p = 100$  bar). These results are a clear evidence for our hypothesis, which proposed the formation of a depletion zone

of cyclohexane close to the surfactants and a cyclohexane-enriched zone at the center of the swollen micelles. A very similar profile can also be observed for the contrast A at  $p = 300$  bar. However, here the increase of SLD is slightly steeper than at  $p = 100$  bar, which is due to the fact that the volume of the micelle decreases with pressure.

The scattering length density profiles of contrast D display a minimum between  $60$  and  $70 \text{ \AA}$ , which stems from the amphiphilic surfactant film. Also here it is obvious that the regime of non-constant scattering intensity stretches over half of the micelle radius. The additional core scattering contribution due to the enrichment of cyclohexane-d12 in the centre of the micelle becomes obvious due to the observation that the scattering length densities of core and bulk are different, i.e.  $\rho_{\text{core}} \neq \rho_{\text{bulk}} \neq \rho_{\text{film}}$ . Note, that the impact of this contrast is discussed with respect to the, at a first sight, special shape of the PDDFs, shown in Fig.8 D.

The actual distribution of  $\text{CO}_2$  and cyclohexane in the centre of the swollen micelle can directly be obtained from the value of the scattering length density at  $r = 0$ . For the contrasts A, B and D it turned out that the fraction of cyclohexane in the centre of the micelles is  $\beta_{\text{core}} \approx 0.5$  and therewith much larger than the value of  $\beta_i \approx 0.2$  obtained for a homogeneous distribution of  $\text{CO}_2$  and cyclohexane. Note, that analyzing the value of SLD( $r = 0$ ) in contrast C  $\beta_{\text{core}} \approx 0.3$  is obtained. A reason for this considerable smaller value of  $\beta_{\text{core}}$  might be the very low scattering contrast. Note that for all contrasts the concentration of cyclohexane at the core increases slightly with increasing pressure.

Taking a closer look at the radial scattering length density (SLD) profiles it becomes obvious that the influence of the pressure onto the SLD at the centre of the micelle, i.e. SLD( $r = 0$ ), seems to be different for the adjusted contrasts. While for the contrast A and C the value of the SLD( $r = 0$ ) at  $p = 100$  bar and  $p = 300$  bar differs only slightly ( $\Delta\text{SLD}(r = 0) = 0.09 \cdot 10^{10} \text{ cm}^{-2}$ ), the difference is much more significant at the contrasts conditions B and D ( $\Delta\text{SLD}(r = 0) = 0.7 \cdot 10^{10} \text{ cm}^{-2}$ ). This behavior can be explained realizing that deuterated cyclohexane-d12 is used for the contrasts B and D, while protonated cyclohexane-h12 is applied for the contrasts A and C. Assuming that an increase of the pressure leads to a slightly higher concentration of cyclohexane at the core (thereby avoiding the increasing repulsive interactions caused by the pressure induced shrinkage of the microemulsion droplets), the increase of the SLD of  $\text{CO}_2$  is partly compensated by the negative SLD of protonated cyclohexane-h12. Using deuterated cyclohexane-d12, in contrast, both the pressure-induced increasing fraction cyclohexane-d12 in the centre of the droplet and the increase of the SLD of  $\text{CO}_2$  leads to a higher value of SLD( $r = 0$ ).

By using the experimentally determined scattering length densities at the centre of the swollen micelle, the values for  $\Delta\rho_{\text{core}}(r = 0)$  can be compared to the ones used for the radial density distribution function  $f_{\text{droplet}}(R)$ . In all cases, the absolute values for  $\Delta\rho_{\text{core}}$  used for  $f_{\text{droplet}}(R)$  are smaller than the ones obtained from the GIFT procedure. The smaller values of  $|\Delta\rho_{\text{core}}(r = 0)|$  can be explained by the fact, that the applied radial density distribution function  $f_{\text{droplet}}(R)$  proposed by Foster<sup>46</sup> is not able to describe the scattering length density profile obtained by the GIFT procedure, i.e. the enrichment of cyclohexane in the micellar core, quantitatively. Reconsidering the analytical form of  $f_{\text{droplet}}(R)$  (see Eq(11)) one easily sees, that the parameter  $\chi$  can only account for symmetric diffusivities. As a consequence the combination of the

respective form factor  $P_{\text{droplet}}(q)$  (see Eq(11)) and polydisperse Percus-Yevick structure factor  $S_{\text{PY}}(q)$  is not able to describe the scattering data recorded at  $q$ -values slightly larger than the position of the oscillation quantitatively (see e.g. Fig. 7D).

Last but not least, comparing the diameter of the droplets obtained from the GIFT procedure with the ones obtained from the fits of the scattering data a good agreement is found.

## Conclusions

Microemulsions containing near or supercritical CO<sub>2</sub> are of interest for both fundamental research as well as technical applications. In this study we discovered an unexpected new way to boost the efficiency of non-biodegradable and therefore environmentally questionable fluorinated surfactants to formulate CO<sub>2</sub>-microemulsions. This efficiency boosting is obtained by the partial replacement of CO<sub>2</sub> by a hydrophobic substance as e.g. cyclohexane. We found, for example, that the substitution of about 20 wt% of CO<sub>2</sub> by cyclohexane reduces the amount of surfactant needed to formulate a one-phase microemulsion by a factor of two to five, depending on the pressure. Thus, we were able to formulate a microemulsion with almost equal volumes of brine and CO<sub>2</sub>/cyclohexane ( $\beta_i = 0.2$ ) using only 11 wt% of the fluorinated surfactants Zonyl FSO 100 and Zonyl FSN 100 at  $p = 300$  bar. However, at first sight this result is surprising because the interaction between cyclohexane and the fluorinated alkyl chains of the surfactants is of repulsive nature. We postulated that the distribution of cyclohexane within CO<sub>2</sub> is not homogeneous but that a depletion zone of cyclohexane close to the surfactants is formed.

In order to verify this hypothesis we performed small angle neutron scattering experiments using the contrast variation technique, which is known to be a powerful tool not only to investigate the microstructure but also the spatial distribution of the various components in microemulsion domains. We adjusted the scattering length density of micelles swollen with the CO<sub>2</sub>/cyclohexane mixture using protonated or deuterated cyclohexane. The scattering length density of the continuous brine phase was adjusted by applying different ratios of H<sub>2</sub>O to D<sub>2</sub>O (see Fig.6). The scattering data recorded at four different pressures and contrasts could be almost quantitatively described using the form factor  $P_{\text{droplet}}(q)$  of polydisperse spherical droplets (see Eq(11)) and the polydisperse Percus-Yevick structure factor  $S_{\text{PY}}(q)$ . Small but systematic deviations were observed for  $q$ -values slightly larger than the position of the oscillation. They already indicate that the used radial density distribution function is not able to describe the distribution of CO<sub>2</sub> and cyclohexane inside the micelle quantitatively.

Applying the Generalized Indirect Fourier Transformation (GIFT) we obtained the pair distance distribution functions (PDDFs) which were subsequently deconvoluted to obtain the radial scattering length density distribution profiles. In all cases, instead of a nearly constant scattering length density, a density profile that varies systematically over half of the droplet radius was found. These results confirm our hypothesis of a concentration gradient within the micelle. While cyclohexane is concentrated in the center of the swollen micelle ( $\beta_{\text{core}} \approx 0.5$ ), it is depleted close to the fluorinated amphiphilic film. Hence, we could elucidate that the observed unexpected efficiency boosting of CO<sub>2</sub>-microemulsions is caused by an improvement of the CO<sub>2</sub>-surfactant interactions triggered through repulsive interactions between cyclohexane and the fluorinated surfactant chains.

## Acknowledgements

We are very grateful to the technical workshop of the Physical Chemistry Department of the University of Cologne headed by H. Metzner who constructed and maintained the high pressure SANS cell. The performed studies were only feasible by their design and handworking skills. Furthermore we would like to thank David Bowyer, technician at the D11 instrument, for fast and very skillful help. We also would like to thank Otto Glatter for help with the analysis of the data applying GIFT. Y. Pütz and L. Grassberger wish to thank the *Fonds der chemischen Industrie* (FCI) for financial support.

## Notes

<sup>a</sup>Department of Chemistry, University of Cologne, Luxemburger Str. 116, D-50939 Cologne, Germany.

<sup>b</sup>Institut Laue-Langevin, LSS Group, 71 avenue des Martyrs, F-38000 Grenoble, France

<sup>c</sup>Institute of Physical Chemistry, University of Stuttgart, Pfaffenwaldring 55, D-70569 Stuttgart, Germany. E-mail: thomas.sottmann@ipc.uni-stuttgart.de; Tel: +49 (0)711685 64494.

† Footnotes should appear here. These might include comments relevant to but not central to the matter under discussion, limited experimental and spectral data, and crystallographic data.

Electronic Supplementary Information (ESI) available: details of any supplementary information available should be included here. See DOI: 10.1039/b000000x/

## References

1. P. Hubert and O. G. Vitzthum, *Angew. Chem. Int. Ed. Engl.*, 1978, 17, 710-715.
2. C. A. Eckert, C. L. Liotta, D. Bush, J. S. Brown and J. P. Hallett, *J Phys Chem B*, 2004, 108, 18108-18118.
3. M. J. Dabney and F. V. Bright, *J Phys Chem C*, 2012, 116, 18340-18346.
4. J. D. Holmes, D. C. Steytler, G. D. Rees and B. H. Robinson, *Langmuir*, 1998, 14, 6371-6376.
5. M. Wang, B. Zhao, S. H. Xu, L. Lin, S. J. Liu and D. N. He, *Chem Commun*, 2014, 50, 930-932.
6. M. C. McLeod, R. S. McHenry, E. J. Beckman and C. B. Roberts, *J Phys Chem B*, 2003, 107, 2693-2700.
7. C. A. Eckert, B. L. Knutson and P. G. Debenedetti, *Nature*, 1996, 383, 313-318.
8. E. Lack, H. Seidlitz and P. Toro, *13th International Scientific Colloquium on Coffee*, 1989, 236-245.
9. K. A. Consani and R. D. Smith, *The Journal of Supercritical Fluids*, 1990, 3, 51-65.
10. M. Schwan, L. G. A. Kramer, T. Sottmann and R. Strey, *Phys Chem Chem Phys*, 2010, 12, 6247-6252.
11. T. A. Hoefling, R. M. Enick and E. J. Beckman, *J Phys Chem-US*, 1991, 95, 7127-7129.
12. K. Harrison, J. Goveas, K. P. Johnston and E. A. Orear, *Langmuir*, 1994, 10, 3536-3541.
13. J. Eastoe, Z. Bayazit, S. Martel, D. C. Steytler and R. K. Heenan, *Langmuir*, 1996, 12, 1423-1424.
14. O. Holderer, M. Klostermann, M. Monkenbusch, R. Schweins, P. Lindner, R. Strey, D. Richter and T. Sottmann, *Phys Chem Chem Phys*, 2011, 13, 3022-3025.
15. M. Klostermann, R. Strey, T. Sottmann, R. Schweins, P. Lindner, O. Holderer, M. Monkenbusch and D. Richter, *Soft Matter*, 2012, 8, 797-807.
16. Y. Takebayashi, Y. Mashimo, D. Koike, S. Yoda, T. Furuya, M. Sagisaka, K. Otake, H. Sakai and M. Abe, *J Phys Chem B*, 2008, 112, 8943-8949.

17. Z. Shervani, Y. Ikushima, Y. Hakuta, H. Kunieda and K. Aramaki, *Colloid Surface A*, 2006, 289, 229-232.
18. K. J. Thurecht, D. J. T Hill and A. K. Whittaker, *Macromol Chem Phys*, 2006, 207, 1539-1545.
19. J. S. Keiper, J. A. Behles, T. L. Bucholz, R. Simhan, J. M. DeSimone, G. W. Lynn, G. D. Wignall, Y. B. Melnichenko and H. Frielinghaus, *Langmuir*, 2004, 20, 1065-1072.
20. M. Sagisaka, S. Iwama, S. Hasegawa, A. Yoshizawa, A. Mohamed, S. Cummings, S. E. Rogers, R. K. Heenan and J. Eastoe, *Langmuir*, 2011, 27, 5772-5780.
21. A. Muller, Y. Putz, R. Oberhoffer, N. Becker, R. Strey, A. Wiedenmann and T. Sottmann, *Phys Chem Chem Phys*, 2014, 16, 18092-18097.
22. J. Eastoe, A. Downer, A. Paul, D. C. Steytlér, E. Rumsey, J. Penfold and R. K. Heenan, *Phys Chem Chem Phys*, 2000, 2, 5235-5242.
23. J. Eastoe, A. Paul, A. Downer, D. C. Steytlér and E. Rumsey, *Langmuir*, 2002, 18, 3014-3017.
24. A. Favrelle, C. Boyere, K. M. Tran, D. Alaimo, B. Calvignac, M. Paquot, F. Boury, C. Jerome and A. Debuigne, *J Colloid Interf Sci*, 2013, 398, 273-275.
25. J. Eastoe, A. Paul, S. Nave, D. C. Steytlér, B. H. Robinson, E. Rumsey, M. Thorpe and R. K. Heenan, *J Am Chem Soc*, 2001, 123, 988-989.
26. S. Cummings, R. Enick, S. Rogers, R. Heenan and J. Eastoe, *Biochimie*, 2012, 94, 94-100.
27. A. Mohamed, M. Sagisaka, M. Hollamby, S. E. Rogers, R. K. Heenan, R. Dyer and J. Eastoe, *Langmuir*, 2012, 28, 6299-6306.
28. M. Sagisaka, D. Koike, S. Yoda, Y. Takebayashi, T. Furuya, A. Yoshizawa, H. Sakai, M. Abe and K. Otake, *Langmuir*, 2007, 23, 8784-8788.
29. A. Mohamed, M. Sagisaka, F. Guittard, S. Cummings, A. Paul, S. E. Rogers, R. K. Heenan, R. Dyer and J. Eastoe, *Langmuir*, 2011, 27, 10562-10569.
30. S. Burauer, T. Sottmann and R. Strey, *Tenside Surfact Det*, 2000, 37, 8-16.
31. M. Kahlweit and R. Strey, *Angew Chem Int Edit*, 1985, 24, 654-668.
32. M. Kahlweit, R. Strey and G. Busse, *J Phys Chem-US*, 1990, 94, 3881-3894.
33. M. Kahlweit, R. Strey, D. Haase, H. Kunieda, T. Schmeling, B. Faulhaber, M. Borkovec, H. F. Eicke, G. Busse, F. Eggers, T. Funck, H. Richmann, L. Magid, O. Soderman, P. Stilbs, J. Winkler, A. Dittrich and W. Jahn, *J Colloid Interf Sci*, 1987, 118, 436-453.
34. M. Klostermann, T. Foster, R. Schweins, P. Lindner, O. Glatter, R. Strey and T. Sottmann, *Phys Chem Chem Phys*, 2011, 13, 20289-20301.
35. L. W. Diamond and N. N. Akinfiev, *Fluid Phase Equilib*, 2003, 208, 265-290.
36. M. Kotlarchyk and S. H. Chen, *J Chem Phys*, 1983, 79, 2461-2469.
37. M. Kotlarchyk, S. H. Chen, J. S. Huang and M. W. Kim, *Phys Rev A*, 1984, 29, 2054-2069.
38. V. Lisy and B. Brutovsky, *Phys Rev E*, 2000, 61, 4045-4053.
39. M. Gradzielski, D. Langevin and B. Farago, *Phys Rev E*, 1996, 53, 3900-3919.
40. J. S. Pedersen, *J Appl Crystallogr*, 1994, 27, 595-608.
41. J. K. Percus and G. J. Yevick, *Phys Rev*, 1958, 110, 1-13.
42. J. Kubelka, R. A. G. D. Silva and T. A. Keiderling, *Biophys J*, 2002, 82, 38a-38a.
43. T. Foster, T. Sottmann, R. Schweins and R. Strey, *J Chem Phys*, 2008, 128.
44. M. Gradzielski, D. Langevin, L. Magid and R. Strey, *J Phys Chem-US*, 1995, 99, 13232-13238.
45. Y. Y. Won, H. T. Davis, F. S. Bates, M. Agamalian and G. D. Wignall, *J Phys Chem B*, 2000, 104, 7134-7143.
46. T. Foster, *J Phys Chem B*, 2011, 115, 10207-10217.
47. R. Bracewell, *Fourier Transform and its Applications*, McGraw Hill, New York, 1986.
48. O. Glatter, *J Appl Crystallogr*, 1977, 10, 415-421.
49. O. Glatter, *J Appl Crystallogr*, 1980, 13, 7-11.
50. J. BrunnerPopela and O. Glatter, *J Appl Crystallogr*, 1997, 30, 431-442.
51. A. Bergmann, G. Fritz and O. Glatter, *J Appl Crystallogr*, 2000, 33, 1212-1216.
52. O. Glatter, *J Appl Crystallogr*, 1981, 14, 101-108.
53. R. Mittelbach and O. Glatter, *J Appl Crystallogr*, 1998, 31, 600-608.
54. J. Brunner-Popela, R. Mittelbach, R. Strey, K. V. Schubert, E. W. Kaler and O. Glatter, *J Chem Phys*, 1999, 110, 10623-10632.
55. M. Kahlweit, R. Strey, R. Schomacker and D. Haase, *Langmuir*, 1989, 5, 305-315.
56. T. Sottmann, M. Lade, M. Stolz and R. Schomacker, *Tenside Surfact Det*, 2002, 39, 20-28.
57. V. H. Dalvi, V. Srinivasan and P. J. Rossky, *J Phys Chem C*, 2010, 114, 15553-15561.
58. V. H. Dalvi and P. J. Rossky, *P Natl Acad Sci USA*, 2010, 107, 13603-13607.
59. M. Kahlweit, R. Strey and G. Busse, *Phys Rev E*, 1993, 47, 4197-4209.
60. K. V. Schubert, G. Busse, R. Strey and M. Kahlweit, *J Phys Chem-US*, 1993, 97, 248-254.
61. P. K. Kilpatrick, C. A. Gorman, H. T. Davis, L. E. Scriven and W. G. Miller, *J Phys Chem-US*, 1986, 90, 5292-5299.
62. F. B. Bombelli, D. Berti, U. Keiderling and P. Baglioni, *Appl Phys Mater*, 2002, 74, S1270-S1273.
63. NIST, scattering length density calculator, <http://www.ncnr.nist.gov/resources/activation/>.
64. M. Gradzielski, D. Langevin, T. Sottmann and R. Strey, *J Chem Phys*, 1997, 106, 8232-8238.
65. B. Weyerich, J. Brunner-Popela and O. Glatter, *J Appl Crystallogr*, 1999, 32, 197-209.
66. R. Strey, O. Glatter, K. V. Schubert and E. W. Kaler, *J Chem Phys*, 1996, 105, 1175-1188.